On demand additive manufacturing of functionally graded concrete

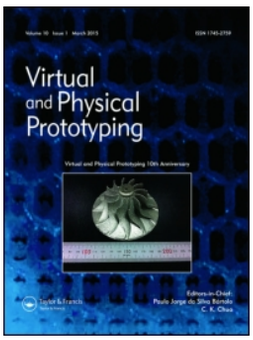

Taylor & Francis
Taylor & Francis Group

Virtual and Physical Prototyping

ISSN: 1745-2759 (Print) 1745-2767 (Online) Journal homepage: https://www.tandfonline.com/loi/nvpp20

On-demand additive manufacturing of functionally graded concrete

Z.Y. Ahmed, F.P. Bos, M.C.A.J. van Brunschot & T.A.M. Salet

To cite this article: Z.Y. Ahmed, F.P. Bos, M.C.A.J. van Brunschot & T.A.M. Salet (2020) On-demand additive manufacturing of functionally graded concrete, Virtual and Physical Prototyping, 15:2, 194-210, DOI: 10.1080/17452759.2019.1709009

To link to this article: https://doi.org/10.1080/17452759.2019.1709009

Published online: 07 Feb 2020.

VIRTUAL AND PHYSICAL PROTOTYPING
2020, VOL. 15, NO. 2, 194–210
https://doi.org/10.1080/17452759.2019.1709009

Taylor & Francis
Taylor & Francis Group

REVIEW

On-demand additive manufacturing of functionally graded concrete

Z.Y. Ahmed, F.P. Bos, M.C.A.J. van Brunschot and T.A.M. Salet

Department of the Built Environment, Eindhoven University of Technology, Eindhoven, Netherlands

ABSTRACT

The rapid development of additive manufacturing of cementitious materials has enabled the emergence of a new design paradigm, namely functional grading of material properties by location. Target performance parameters could be material weight and insulation value or (particularly important) ductility. A generic concept to achieve this, is through the selective addition of fibres or aggregates. In 3D concrete printing (3DCP), this concept can be developed into two strategies: by adding particles (i) to the bulk mixture through a second stage mixing process at the printer head (*Simultaneous Process*, SP), or (ii) in between the layers of deposited cementitious filament (*Repetitive Sequential Process*, RSP). The present paper presents the development of specific equipment required to obtain on–demand functional grading of the printed material. Subsequently, the application of these systems in print trials is shown. The current study focussed on ductility by creating fibre–reinforced 3D printed concrete through both strategies. The mechanical performance of the obtained material has been established through compressive, flexural, and crack–mouth opening displacement tests. To underline the generic nature of the strategies, a trial with lightweight aggregates has also been performed. It was shown that particularly the SP is capable of achieving improvements in ductility and self–weight.

ARTICLE HISTORY
Received 23 September 2019
Accepted 20 December 2019

KEYWORDS
3D concrete printing; additive manufacturing; on-demand; functional grading; fibres; cementitious materials; process; nozzle

1. Introduction

The development of additive manufacturing of cementitious materials (AMoC) is rapidly gaining traction, both in terms of scientific research as in in-practice projects. An extensive overview of the developments in the field is given by (Wangler et al. 2019) [the reader may also refer to (Camacho et al. 2018; Tay et al. 2017) to obtain an impression of research progress], whereas recent in-practice projects include a pre-stressed bridge 3D concrete printed bridges in the Netherlands (Salet et al. 2018; Material district 2019), highly intricate 3D concrete printed columns by ETH Zurich (Aouf 2019), prototypes for 3DCP houses (Aouf 2018; Jordahn 2018) and pavilion (Mensley 2017).

Introduction of this family of digital manufacturing technologies has also enabled the emergence of a new design paradigm for the objects they create, namely on-demand functional grading (OD-FG) of properties by location. It was first introduced by prof. Salet as the 'Colour Printer' for 3DCP, in a key-note address to the 2nd International Conference on Progress in Additive Manufacturing in Singapore and elaborated by (Bos et al. 2016): considering (i) a print head, through the very nature of the process, builds an object by passing through each point of the object and assuming (ii) the print head is capable of grading the properties of the deposited material during printing, it follows that, within the available material grading range, the object can be designed to meet performance requirements customised by location and manufactured in a continuous and single-stage process. Target performance parameters for functional grading in concrete could be material weight and insulation value, conductivity, self-healing ability, the introduction of sensors for various monitoring and quality control, and self-cleaning capabilities. A particularly important performance characteristic that could be subjected to functional grading is ductility and tensile strength because the lack of suitable reinforcement methods has been identified as a major obstacle in the development of this technology (Asprone et al. 2018).

A range of AMoC technologies is currently under development, including stereo-lithography (STL) inspired powder-bed printing (Lowke et al. 2018), (adaptive) sliding formwork [e.g. Smart Dynamic Casting (Lloret et al. 2015)] and selective material deposition by spraying

CONTACT Z.Y. Ahmed z.y.ahmed@tue.nl Department of the Built Environment, Eindhoven University of Technology, P.O. Box 513, 5600 MB Eindhoven, Netherlands

[e.g. Shotcrete 3D Printing, SC3P (Lindemann et al. 2018)]. Currently, the most common variant is that of extrusion-based layering of filaments, often referred to as 3D concrete printing (3DCP) (Bos et al. 2016). The current study applies to this technology in particular.

Although the paradigm of functional grading has been introduced to other 3D printing technologies, remains practically untouched from a 3DCP process perspective. Therefore, the current study seeks to present an initial proof-of-concept for OD-FG of printed concrete, primarily aimed at ductility characteristics (in the context of this study to be read as with or without), but on a generic basis for multiple applications, as shown by grading of specimen density.

2. Functional grading in 3DCP

2.1. Functionally graded materials (FGMs)

Functionally Graded Materials are characterised by a gradual transition of properties by location. FGMs result in superior behaviour compared to multi-materials and composites, in which discrete changes between materials, and thus properties, occur (Leung, Mao, and Chen 2018).

A wide range of material properties can be gradient throughout a material, including density, strength, rigidity, impact resistance, thermal and acoustic insulation, conductivity, etc. In nature, it is a common phenomenon that allows optimised use of materials and thus energy, for instance in bone structures (Audibert et al. 2018). But the definition can apply to a host of non-related, very different materials, ranging from polymers to metals to ceramics. Likewise, functional grading can be achieved through many different mechanisms, including variations in (chemical) material composition and (micro-) structure. Depending on the mechanism, the geometrical scale over which the grading occurs can thus also vary significantly.

The concept of applying functional gradients in engineering materials was already introduced in the early 1970s (Bever and Duwez 1972; Shen and Bever 1972), but due to the complexities involved in manufacturing such materials, actual applications only started to be developed from about a decade later.

Additive manufacturing turned out to be a manufacturing concept that, in comparison to other approaches such as forming and subtraction, is relatively well-fitting to produce FGMs, due to its specific nature of localised control over the build-up of objects.

As a consequence, several variants of 3D printing Functionally Graded Materials (FGMs) have now become common. For instance, by using two different base materials of which the proportions can vary from 0-100% to 100-0% for each voxel, Fused Deposition Modelling (FDM) polymer 3D printers have been shown to be capable of producing objects with significantly graded rigidity (Altenhofen et al. 2018; Garland and Fadel 2015). In powder-bed steel printing, different powders of pure metals or alloys can be used by layer to achieve functional grading (Kirk et al. 2018). Local Composition Control (LCC) (where composition control refers to the material density, rather than the chemical composition) has also been introduced, particularly to optimise the inside volume of objects printed through powder-bed based 3D printing methods (Cho et al. 2002). Developments of Functional Grading and Multi-Material Additive Manufacturing (MMAM) are continuing, as shown by (Mohammad et al. 2013).

However, although FGMs is an established notion in several production industries, this concept has hardly been applied in the construction-oriented concrete industry. Outside the domain of AM, a few studies have reported on cast concrete with graded ductility by locally using (different types of) fibre reinforcement (Shen et al. 2008; Maalej, Ahmed, and Paramasivam 2003; Plückelmann, Song, and Breitenbücher 2017). But although it was already suggested in (Mohamed and Li 1995), that this could be an approach to efficient structural concrete element design, the idea never found widespread application, probably due to the complex manufacturing of such members.

With the recent developments in AMoC, though, the concept of FG is likely to achieve more success, as production hurdles are being eliminated. Indeed it has been identified as a future research topic (Tay et al. 2017) and some fledgling examples have been presented. Oxman, Keating, and Tsai (2011) published results on small samples of printed Portland cement in which the density had been graded by controlling the addition of an aluminium and lime powder admixture. Craveiro, Bártolo, and Bártolo (2013) presented a FGM printing concept for the construction industry based on the use of two nozzles for different materials and showed a small sample with two different polyurethanes. Their concept results more in a multi-material composite than a true FGM, but on the scale of a building and required performance grading rate (i.e. performance change over distance), this difference could become irrelevant. More recently, Craveiro et al. (2017) developed a computational tool to design functionally graded building components based on the concept of a wall from concrete mixed with different types and quantities of lightweight aggregates per voxel. This work was purely analytical and computational and did not discuss the actual manufacturing of such graded material. Bao

et al. (2018) studied the structural and purification performance of small Engineered Cementitious Composite (ECC) slabs, in which titanium oxide TiO_2 was added to the mixture throughout either the full or part of the slab. The assumption was that such grading could be achieved through extrusion-based concrete printing processes, but in that particular study consecutive manually operated caulk guns, loaded with the two different mixtures, were used. Possibly the most advanced example of actually additively manufactured FGM on building component scale was introduced by Duballet, Gosselin, and Roux (2015). They presented a fully integrated system for both the digital design and actual manufacturing through extrusion-based filament printing of a cementitious mortar in which polystyrene beads can be mixed at the print head through a screw dosage system, in a volume percentage of up to 100% (pure beads, no mortar). It may thus be clear that, although FG by AM has been an established concept in several manufacturing industries, it has hardly been developed for the construction industry.

2.2. 3DCP functional grading concept and strategies

Before introducing the applied FG concept and strategies, integration into the continuous printing process should be recognised as an important boundary constraint. To maintain the advantages of 3DCP, the process should not be disrupted by conflicting intermediate or post-processing actions. The applied concepts and strategies were developed with consideration of this requirement.

A generic concept to accomplish functional grading of material properties in concrete is through the addition of solid discrete particles, such as various types of fibres or aggregates. This is a universal principle to create concretes with different properties, although generally in a continuous rather than a graded composition. This approach is similar to those applied by Bao et al. (2018) and Duballet, Gosselin, and Roux (2015), but expands on it as it aims not to be constrained to the variation of a single type of particle. Alternative concepts could include the addition of gaseous or fluid admixtures (Oxman, Keating, and Tsai 2011), but are outside the scope of the current study.

In the context of extrusion-based concrete printing as applied in the current study, two strategies are proposed to apply the concept of discrete particle addition. These can be applied independently or jointly:

i Adding particles to the bulk mixture through a second stage mixing process at the printer head with a simultaneous process (Duballet, Gosselin, and Roux 2015) or
ii Adding particles in between the layers of deposited cementitious filament with a repetitive sequential process.

The latter strategy is a novel approach enabled by the layering character of the adopted process. This strategy has the distinct advantage that it does not affect the properties of the print mortar itself and does not require complex 2nd stage mixing – although it does introduce other considerations, as will be discussed in Section 5.2.

3. Development of 3DCP subsystems

The present study was performed on the 3DCP facility of the [anonymous], extensively described in Bos et al. (2016), which is based on the layered-extrusion technology pioneered by Khoshnevis with Contour Crafting (Khoshnevis 2004; Khoshnevis et al. 2001, 2006) and similar to the set-up used by University of Loughborough (Lim et al. 2012). One-phase printable mortar Weber 3D 145-2, was used as the base material. As additive particles, Fibraflex FF/15E0 fibres were used to the majority of the study (Fibraflex Brochure, n.d.) and complemented with additional tests with lightweight aggregate.

To achieve either of the suggested strategies required the development of specific equipment capable of three tasks:

a delivering the required particles to the (moving) print head in constant quantities, and
b (strategy 1, Simultaneous process, SP) mixing the particles into the base material at the print head, and subsequently printing the mixed material, or
c (strategy 2, Repetitive sequential process, RPS) depositing the particles onto the printed layers immediately once the layers are printed.

Two subsystems were designed: the Particle Transportation System (PTS) to perform tasks (a) and (c) and the 2nd-stage Particle Addition Device (PAD) for task (b). Figure 1 provides a schematic drawing of the TU/e 3DCP facility with both the new subsystems indicated.

3.1. Airborne particle transportation system (PTS)

Both grading strategies require the designated particles to be available at the print head. For the first strategy (of adding particles in the mortar), it would theoretically be possible to apply the particles during the 1st stage mixing in the mixer-pump outside the print box.

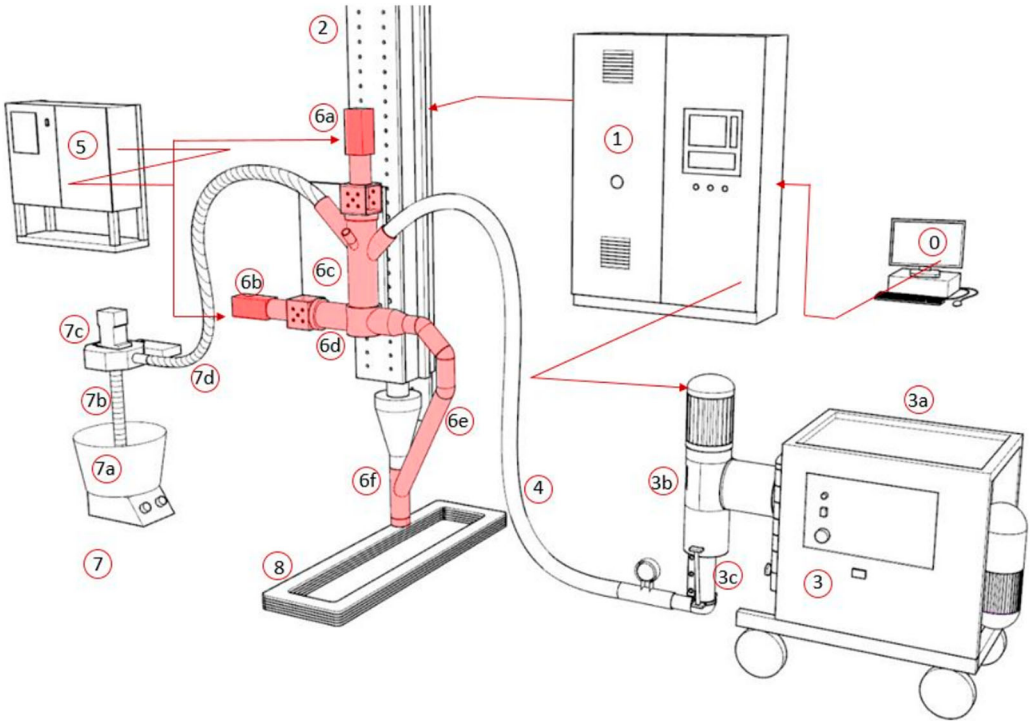

Figure 1. 3DCP set up with the Simultaneous Process (SP) for fibre deposition using the PAD system at Eindhoven University of Technology. 1. Sinumerick robot controller, 2. Gantry robot, 3. Concrete pump, 3(a) Dry Mixing chamber, 3(b) Wet concrete chamber, 3(c) Rotor stator pump, 4. Concrete hose, 5. Controller for mixing and pumping motors of PAD, 6(a). Mixing motor, 6(b). Pumping motor, 6(c). Mixing Chamber, 6(d). Pumping Chamber, 6(e). secondary hose, 6(f). Printing tool with nozzle, 7(a). Vibration bucket, 7(b). Input hose, 7(c). Suction and blower device, 7(d). Output hose (including splitter, left out in this image for reasons of clarity), 8. 3D printed concrete layers.

However, this would considerably complicate the print planning as the delay between particle addition and actual deposition at the print head would have to be taken into account. More importantly, though, the linear displacement pump only allows the use of very small particles in the mixture, typically ≤ 2 mm in diameter.

Particles can be made available at the print head by storing them in a local container (Duballet, Gosselin, and Roux 2015), or by continuously transporting them from a detached reservoir outside the print box to the print head. The former has a distinct advantage that no additional transport mechanism is required but weight and size of such a container is likely to be restricted by the robot payload. Thus, the concept seems unsuitable for large scale continuous processes. The feasibility of a continuous supply system should, therefore, be explored. The lack of such a system instigated the development of the Particle Transportation System (PTS) applied in this project, which needed to fulfil the following requirements:

- capable of transporting the desired particles,
- not interfere with the existing setting of the print facility at [anonymous],
- continuously and steadily delivering the particles in their target quantities,
- adjustable to customise the particle quantities by location.

To achieve this, an airborne system is proposed. The particles are sucked out of a reservoir, transported through a flexible hose and delivered to the print head. Particularly the requirements with regard to freedom of movement and degrees of freedom seem to be hard to achieve with other transport mechanisms such as conveyor belts.

3.1.1. Design

The overall design of airborne PTS is detailed in Figure 4. The particle reservoir (1) consists of a bucket equipped with a slightly curved bowl at the bottom, placed on a vibrating machine (Figure 2a, 3a). Two rods sticking through the bottom fix the bucket to the vibrating table and provide a fixture for a steel clamp that fixes the input hose at a predetermined height from the bowl surface. In the current state of development, the particles are added to the bucket by hand. However, this could be automated by applying standard delivery

Figure 2. Various parts of the airborne PTS system, *(a). Vibration bucket and Input hose, (b). Suction and blower chamber, (c) Rotor blade in blower chamber*.

systems. The bowl curvature, in combination with the constant vibrating of both the bucket and the input hose, ensures a rather constant particle flow (i.e. quantity of particles transported per unit time), while clogging is avoided.

The actual transportation is provided by a 2000 watts servomotor (Figure 2(b)) operated with a steel blower blade (4) (section geometry provided in Figure 2(c)) that sucks the particles out of the reservoir through the input hose and blows them into the transportation hose. Both hoses are made out of polyurethane reinforced with copper-plated steel spiral, with the input hose having a diameter of 60 mm and the output hose diameter of 50 mm. The transportation hose length is 5 m (to allow sufficient movement of the printer head), while the input hose is approximately 1 m long. The particle flow depends on a number of parameters, including the particle type (size, geometry, weight), bucket vibration frequency, input hose height above the bowl $h_{hose,in}$, hose characteristics (diameter, material, surface), blade geometry, and the suction force, which in turn is a function of the blade rotation speed. Of these, the bucket vibration frequency and the suction blade rotation speed are readily controllable by adjusting the regulators for power intake in the vibration device and the servomotor (which is equipped with a step-less turning knob), respectively. Optionally, the input hose height may also be adjusted. The other parameters are fixed for this device or the selected particle.

At the end of the transportation hose, a three-way splitter is mounted (shown in figure 4a). The main function of this part is to reduce the air pressure that is exerted on the print filament or into the PAD. It also reduces the amount of fibres in or onto the concrete (see discussion in subsequent subsection). Only one of the three exit branches of the splitter was used to supply particles. The other two exit branches are emptied into additional reservoirs that can be used to assess the amount of particles inserted into the PAD or between the layers (by averaging their collected quantities).

3.1.2. Selection of fibres and other particles

A test programme was conducted to evaluate the suitability of various fibres and other particles to be transported through the developed airborne-based system. Twenty fibres for structural use purposes obtained from a range of manufacturers, as well as a lightweight aggregate, were assessed on suitability. Initially, it was tested whether the particles could be transported without getting (severely) damaged. Out of the fibres that met both these criteria, a selection was made based on expected structural performance, processability and further practical criteria, to test whether a sufficient and consistent quantity could be transported (further discussed in Subsection 3.1.3). The results are listed in Table 1.

In this context, damaged was perceived as a visually observable change to the fibre that would be likely to severely limit its structural performance. As the various fibres operate on the basis of different principles, this could entail a number of occurences. In the Dramix 3D fibres, straightening of the end hooks, which govern pull-out resistance, was sometimes observed. For three

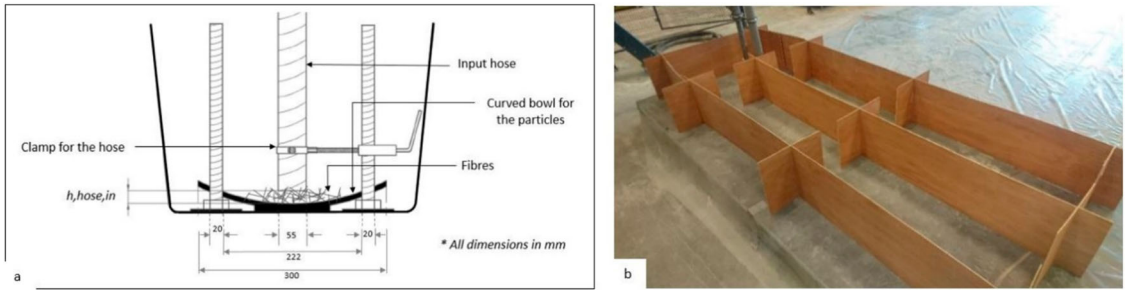

Figure 3. (a) Detailed cross-section of the vibration bucket, (b) segmentation around the print path for fibre collection from PTS system.

Table 1. Suitability performance of fibres and other particles while trial testing in the PTS.

Fibre (or particle)	Shape	Material	Length [mm]	(eq.) Diameter [mm]	Transport-table? [Y/N]	Undamaged? [Y/N]	Sufficient and consistent? [Y/N]
Dramix OL 6/.16	Straight	HS steel	6	0.16	Y	Y	n/a**
Dramix OL 13/.20	Straight	HS steel	13	0.20	Y	Y	n/a**
Dramix 3D RC-4530-BL	Hooked-end	HS steel	30	0.62	Y	N	n/a
OL 6530 Proef 9635E	Crimped	HS steel	20	0.30	Y	Y	n/a
Synmix SP55	Waved	Polymer type II	55	0.85	N	n/a	n/a
Duomix M12	Straight	Polymer type IA	12	0.03	Y	N	n/a
Fibraflex FF/30L6	Flat	HS steel	30	0.029	Y	Y*	n/a
Fibraflex FF/20L6	Flat	HS steel	20	0.029	Y	Y*	Y
Fibraflex FF/20E0	Flat	HS steel	20	0.024	Y	Y*	n/a
Fibraflex FF/15E0	Flat	HS steel	15	0.024	Y	Y*	Y
Fibraflex FF/10E0	Flat	HS steel	10	0.024	Y	Y*	n/a
Fibraflex FF/5E0	Flat	HS steel	5	0.024	Y	Y*	n/a
Turbobuild dispergate AC-12-300/D	Straight	Basalt	12	0.04	Y	N	n/a
Turbobuild integral AC 24-200/I	Straight	Basalt	24	0.12	Y	Y	n/a
Uncoated chopped fibre	Straight	Basalt	12	0.09	Y	N	n/a
OC reinforcements, Anti crak HP 18	Straight	AR glass	18	0.16	Y	Y	n/a
OC reinforcements, Anti crak HP 24	Straight	AR glass	24	0.44	Y	Y	n/a
OC reinforcements, Anti crak HP 67/36	Straight	AR glass	36	0.54	Y	Y	n/a
Cem-FIL Minibars 24 mm	Twisted	AR glass + resin	24	0.70	Y	Y	Y
Cem-FIL Minibars 43 mm	Twisted	AR glass + resin	43	0.70	N	n/a	n/a
Lightweight aggregate (Liaver balls)	Random shaped granular	Glass granulate	–	5–15	Y	Y	Y

*A limited amount of fibres was chopped, but this was deemed within acceptable limits.
**Discontinued as these needle-type fibres were no longer considered safe for use.

other types of fibres, the wires unbundled. Approximately 20–40% of all types of Fibraflex fibres experienced limited chopping by the rotor blade. However, this was not directly considered prohibitive as it does not fully eliminate the structural capacity of the fibre. Further capacity performance testing was hence performed on two Fibraflex fibres (a longer FF/20L6, and a shorter FF/15E0), as well as on a Cem-FIL glass fibre.

3.1.3 Capacity testing

Two further trial tests have been performed to assess the transportation capacity and consistency of the PTS. Target particle quantities in concrete are usually expressed in mass-to-volume ratio r_m [kg/m^3 ≡ 10^{-6} g/mm^3] (i.e. as mass of particles to volume of matrix, this expression is commonly applied for steel fibres), or VOL% (most other particles). For the use in concrete printing, the values have to be recalculated into mass per unit time (flow) $m'_{particle}$ [g/s], which can be obtained from the print speed v_{nozzle} [mm/s] and nozzle opening A_{nozzle} [mm^2] (assuming $A_{nozzle} \approx A_{filament}$), the particle density $\rho_{particle}$ [kg/m^3 ≡ 10^{-6} g/mm^3], and the target quantities, through either: $m'_{particle} = v_{nozzle} \cdot A_{nozzle} \cdot \rho_{particle} \cdot \text{VOL\%}$, or: $m'_{particle} = v_{nozzle} \cdot A_{nozzle} \cdot r_m$.

The Fibraflex FF/20L6 and FF/15E0 both have a density of $\rho = 7.25 \times 10^{-3}$ g/mm^3 and a target mass-to-volume ratio $r_m = 40 \times 10^{-6}$ g/mm^3 according to the products' declaration of performance (Declaration of performance n.d.) . This yields $m'_{particle} = 100$ mm/s (40·10) mm^2 · 40×10^{-6} g/mm^3 = 1.6 g/s. For the Cem-FIL minibars 24 mm ($\rho = 2.0 \times 10^{-3}$ g/mm^3), no specific target quantity is provided by the supplier, but Crack-Mouth Opening Displacement (CMOD) test results are given for $r_m = 5 \times 10^{-6}$ g/mm^3 to $r_m = 25 \times 10^{-6}$ g/mm^3 for the 43 mm version (Cem-fil Minibars data sheet n.d.), which indicate slightly strain hardening behaviour can be obtained with the highest quantity. This corresponds to $m'_{particle} = 100$ mm/s · (40 × 10) mm^2 · 25×10^{-6} g/mm^3 = 1.0 g/s. A further evaluation of the appropriateness of the given target mass-to-volume ratios falls outside the scope of the current study.

During the trial test, the PTS was operated and the transportation hose was connected to a custom-designed reservoir that allowed air to escape whilst maintaining the fibres. The weight of the output quantity of fibres was measured several times for time intervals of 15, 30, and 60 s, with settings of the power supply ranging from 50 to 300 W, to the servomotor which was registered through a standard wattage metre between motor and the wall socket. It was found that when the blower power is too low (i.e. beneath approximately 100 W), the airflow was insufficient to keep enough fibres airborne. As a result, fibres fell flat in different parts of the PTS. The system became highly dependent on the curvature in the hose and the output was insufficient. On the other hand, when the blower power is increased over a certain limit (for the FF/20L6 fibres around 200 W), too many fibres are sucked in which clogs the PTS, or would likely jam the PAD or cover the complete interlayer surface when

applied between filament layers. With a blower power of 150 W, $h_{hose,in}$ = 25 mm,(Figure 3(a)) and a vibration knob setting of 40 Hz, a relatively consistent flow of $m'_{particle} \approx 2.3 \pm 0.3$ [g/s] was obtained. Although this was above the target quantity, it was not possible to reduce the blower power further for reasons described above.

In a subsequent experiment, the PTS was connected to the print robot and used to move around a rectangular path that was divided into sections (Figure 3(b)). The transportation hose exit was maintained 200 mm above the print surface, in order to avoid the airflow influencing the (fresh concrete) surface. After the robot had completed the path several times, the fibres in each section were collected and weighed. The test was performed 5 times for each fibre, with different blower power settings. In general, it was found that, probably due to motion effects, the scatter in delivered fibres increases in comparison to the static system testing. However, the overall deposition remained approximately the same with the same system settings.

Considering the trial test results, a splitter was introduced to reduce both fibre quantity and air pressure at the PTS output. Additional tests were performed to verify an equal distribution between each of the outputs of the splitter. The most consistent results were achieved when the splitter is attached vertically (as in the illustrations).

In these series of trail tests, it was furthermore observed that the FF/20L6 (contrary to previous assessment from the fibre selection tests), sustained too much damage. Their use was therefore discontinued in the rest of the study.

3.2. 2nd stage particle addition device (PAD)

3.2.1 Design

Figure 4(a) shows an exploded illustration of the complete PAD system, while Figure 4(b) focuses on the mixing-pumping unit of the PAD with the dimension details. The overall system of PAD with PTS is shown in Figure 5. Essentially, it consists of two chambers: one for mixing (7) and one for transporting (9). The wet mortar enters the vertical mixing chamber from the concrete input connection (6), opposite to which the PTS input is located from which fibres or other particles are inserted. The mortar and particles are mixed by a

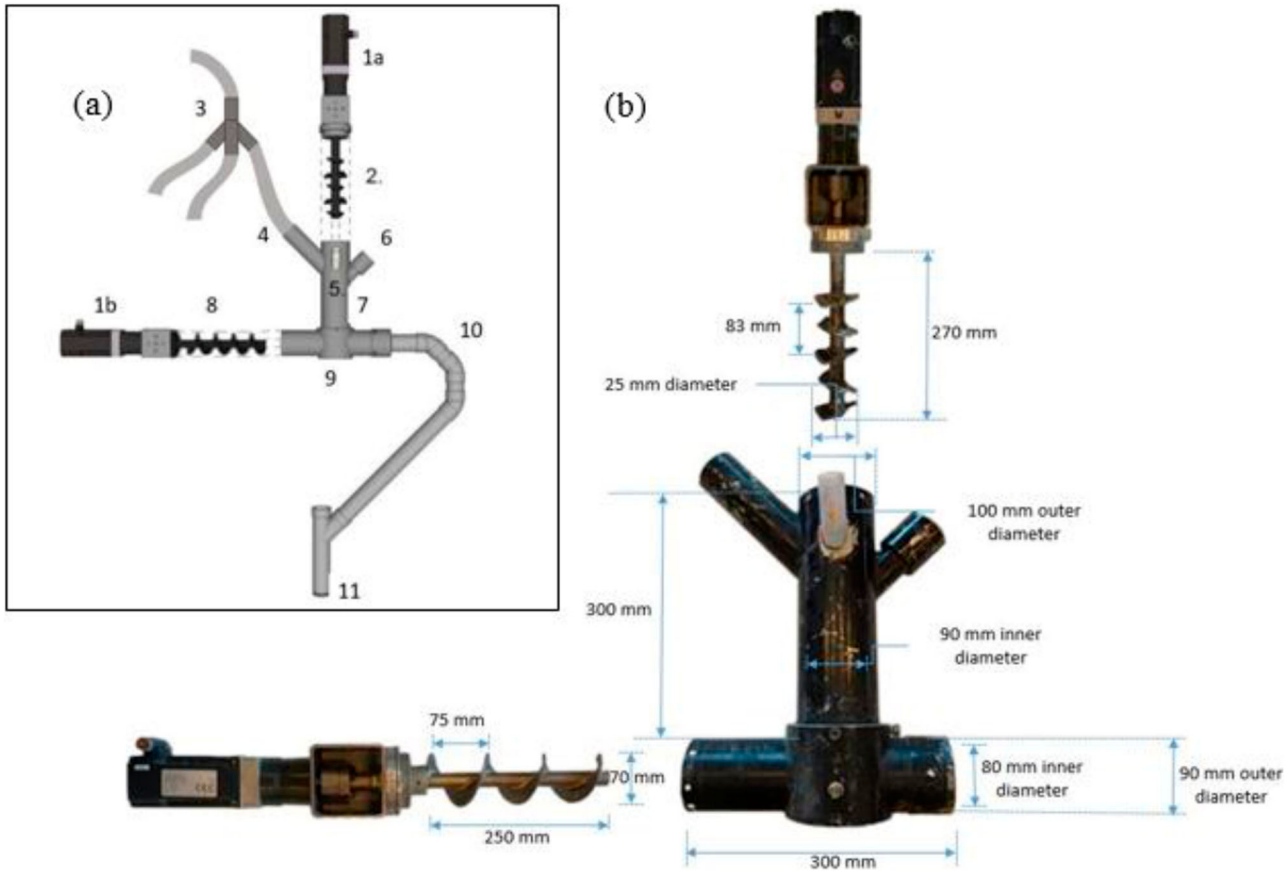

Figure 4. (a) Mixing and pumping device *1(a). Mixing motor, 1(b). Pumping motor, 2. Paddle mixer, 3. Splitter, 4. Additives (fibre/aggregates) vent, 5. Over flow vent, 6. Concrete vent, 7. Mixing chamber, 8. Archimedes screw, 9. Pumping chamber, 10. Secondary Hose, 11. Output nozzle.* (b) Mixing and Pumping unit of PAD in detail, showing the dimensions of the each of the parts.

Figure 5. Shows the setuxp of the PAD system with PTS system.

custom-designed paddle mixer driven by a Beckhoff AM8032-0E10-1000 servomotor. The mixing chamber has an overflow (5), which also serves an air outlet. From the mixing chamber, by gravity and pressure generated by the downward oriented paddle mixer blades, the mixture enters into the horizontal transportation chamber where an Archimedes screw builds the pressure to press the material through the final output pipe to the print nozzle. Like the paddle mixer, the screw is driven by a Beckhoff AM8032-0E10-1000 servomotor. Although the screw cannot generate a high pressure (compared to the linear displacement pump used in the base mixer-pump), it is sufficient to transport the material as the last pipe is only short. Care has to be taken, however, that the internal resistance of the output part remains as low as possible, for instance by avoiding sharp corners and using a smooth piping material. To obtain a constant and sufficient material flow, several settings have to be carefully tuned: the water inlet and pump frequency of the base mixer-pump, the paddle mixer and screw pump frequencies of the PAD, and the print head speed. In the [anonymous] 3DCP facility, the print head speed and mixer-pump settings are controlled by the central Sinumerik operating software. The PAD servomotor settings can be adjusted stepless from 0 to 540 rpm (revolutions per minute) through a touch screen interface connected to the operating system in a control box outside the print box. The system settings have to be tuned for each mortar/particle mixture.

Table 2. Initial settings determined from system testing, for Weber 3D 145–2 mortar with Fibraflex FF20L6 or FF15E0

Parameter	Setting	Parameter	Setting	Parameter	Setting
Base w/b ratio	0.15	M-Tec 2000 pump frequency	20.1 Hz	Print speed	80 mm/s
Input hose height	25 mm	PAD screw pump frequency	348 rpm	Nozzle height PAD	12 mm
Blower power	150 W	PAD paddle mixer frequency	84 rpm	Layer offset	11.5 mm

The PAD system is mounted on an aluminium plate, which in turn is fixed to the vertical arm of the 3DCP gantry robot. The concrete and PTS hoses can then be connected to the appropriate inlets. In the current state of development, particularly to avoid excessive friction in the output part, the default print head with rotating rectangular nozzle is not used. Rather an open round pipe of diameter $d = 35$ mm serves as print nozzle. By using a round nozzle, the need for it to rotate tangential to the print path is obviated, thus significantly reducing the mechanical complexity of the outlet part.

3.2.2 Integrated system testing

The PAD was assessed by stepwise testing of the device, initially without additional particles and without output piping. Subsequently, an output hose was added but replaced with a smoother pipe due to friction-induced blockages. Finally, the operability of the full system with both the PTS and the PAD was tested successfully with FF/15E0 fibres. The primary observation was the necessity to increase the water-to-binder ratio in the mortar from 0.15 to 0.17, in order to maintain the workability once the fibres are added. Table 2 lists the deducted system settings.

4 Experimental evaluation of functional grading with SP: in the bulk material

The developed equipment was used with the TU/e 3DCP facility to explore the ODFG strategy of adding particles

to the bulk print mortar. Fibre-reinforced concrete was printed with two different types of fibres, and mechanically tested. To show the versatility of the system, an additional experiment was performed with lightweight aggregates. The achievable variations in overall density were recorded. Hence, it was shown that the PTS-PAD system can be used to achieve grading of different performance characteristics (in this case, the material density and ductility).

4.1 Methods

Rectangular objects were printed using the PTS-PAD system with the [anonymous] 3DCP facility. Weber 3D 145–2 print mortar was used as the matrix material. Three different particles were added: Fibraflex FF15E0 high-strength steel fibres, Cem-FIL minibars 24 mm alkali resistant glass fibres, and Liaver 4–8 mm expanded glass light weight aggregates (Liaver balls Brochure n.d.). The addition of light weight aggregate was steadily reduced in two steps to obtain three levels of density. For reference, specimens without additional particles were also produced, as were (for some cases) cast specimens. Cast specimens were produced by collecting material directly from the print nozzle opening into standard moulds.

Further settings, including the water-to-mortar ratio, were adjusted to ensure operability of the system and printability of the particle enhanced mortar. Table 3 lists the applied settings for each of the fibre types, as well as for the lightweight aggregate. After printing, the objects were cut into large pieces and covered in foil. After one day of curing under foil, the pieces were removed from the print bed and sawn into specimens of a nominal size of $40 \times 40 \times 40$ mm^3 or $40 \times 40 \times 160$ mm^3, depending on the type of experiment. They were further cured in water until the day of testing.

Cast and printed specimens without and with Fibraflex FF15E0 high-strength steel fibres were subjected to 3 mechanical tests: compressive cube strength, flexural bending test and crack-mouth opening displacement (CMOD). The printed specimens were tested in two directions, namely directions I (parallel to the print direction) and III (vertically perpendicular to print direction, as defined by (Wolfs, Bos, and Salet 2019). Printed specimens with Cem-FIL minibars 24 mm glass fibres were subjected CMOD testing, in direction I. Printed specimens with Liaver (5–15) mm diameter expanded glass light weight aggregate, as well as all other specimens were measured and weighed to determine their density. By adding these aggregates to the mixture, the density of the material can be changed over the length of the print path. In order to quantify this the weight of the specimen printed with light-weight aggregates is compared to that of plain concrete and fibre-reinforced concrete.

The compressive tests were performed according to NEN-EN 12390-3 (NEN-EN 12390-3:2009 EN 2009) on an Automax compression bench from Controls, at a rate of 960 N/s (load-controlled). The flexural tests were performed as 3-point bending tests according to NEN-EN 196-1, on the same bench, at a rate of 50 N/s (load-controlled). The CMOD tests were performed according to NEN-EN 14651 (NEN-EN 14651:2005 EN 2005) but on scaled down specimens (Bos, Bosco, and Salet 2019) have extensively argued this is allowable. The loading rate was controlled by the crack mouth opening, at 0.05 mm/min until a CMOD of 0.1 mm is reached and at 0.2 mm/min until the end of the test (either specimen fracture or when a CMOD of 4.1 mm was reached).

4.2 Results and discussion

4.2.1 Compressive strength

The average results of the compressive test are listed in Table 4 and shown in Figure 6a. The performance of the cast specimens is almost identical to results reported by Wolfs, Bos, and Salet (2019), while the performance of the printed specimens is slightly better. The addition of fibres seems to cause a minor decrease in strength for the cast specimens. In the print specimens, a modest increase in strength is found – most notably in the direction I specimens, which can be explained by the fact that the fibres are oriented in the direction of the complementary tensile forces perpendicular to the compression due to the filament flow during printing.

4.2.2 Flexural strength

The average results of the flexural test are listed in Table 5. In comparison to Wolfs, Bos, and Salet (2019), the

Table 3. PTS-PAD and other system settings; resulting particle quantities.

Particle	PTS settings	PAD settings		3DCP facility settings	
	Blower power	Mixer frequency	Pump frequency	Water to mortar ratio	Nozzle speed
None	–	84 rpm	348 rpm	0.15	60 mm/s
FF15E0	150 W	84 rpm	348 rpm	0.17	60 mm/s
Cem-FIL mb 24 mm	180 w	84 rpm	320 rpm	0.175	60 mm/s
Liaver aggregates	100 W	80–85 rpm	320–340 rpm	0.165	60 mm/s

Table 4. Results of compression test.

Production and orientation	Fibre	Number of specimens	Age at testing	Average compressive strength (rel. stand. dev.)	Results of Wolfs, Bos, and Salet 2019 (average)
Cast	None	5	13 days	41.7 MPa (4.8 %)	42.3 (7 days)
Printed, dir. I	None	10	13 days	33.8 MPa (13.3 %)	29.2 (7 days)
Printed, dir. III	None	10	13 days	34.9 MPa (6.7 %)	28.5 (7 days)
Cast	FF15E0	5	13 days	38.0 MPa (4.6 %)	–
Printed, dir. I	FF15E0	10	13 days	40.3 MPa (5.2 %)	–
Printed, dir. III	FF15E0	10	13 days	36.6 MPa (4.1 %)	–

performance of the cast specimens was inferior. This could be due to fact that these specimens were not compacted by vibration. The printed specimens, on the other hand, perform slightly better, which may be attributed to unidentified process variations. The addition of fibres improves the performance of all series, but the strength increase is the least in the printed specimens in direction III, as the fibre orientation is generally perpendicular to the tensile stresses. For the printed specimens in direction I, the average strengths increases most, by 31%, due to favourable fibre alignment.

4.2.3 Ductility (CMOD)

Table 6 gives an overview of the results of the CMOD tests. Besides the cracking strength f_t, it indicates the scaled CMOD values (Bos, Bosco, and Salet 2019), and the classification of residual strength according to the *fib* Model Code 2010 (International Federation for Structural Concrete (fib), 2013) (based on scaled values). The flexural stress was calculated through $\sigma = \frac{3Fl}{2bh_{sp}^2}$, as indicated by the EN 14651. Figure 7a provides a comparison of average stress-CMOD curves for FF15E0 fibre-reinforced concrete under different orientations, whereas Figure 7b provides a comparison of average stress-CMOD curves in direction I for two different fibres (FF15E0 and CEM-FIL minibar 24 mm fibres), and without fibre.

In the CMOD test, specimens printed without fibres, cast with FF15E0 fibres, and printed with FF15E0 fibres both in directions I and III all showed lower cracking strengths than in the flexural tests. This is the result of peak stresses around the tip of the notch. This effect seems to be strongest in the printed specimens in direction III with FF15E0 fibres. The notch is situated exactly in the layer interface, which may be more sensitive to peak stresses than the bulk material.

As expected, this series (printed, FF15E0 fibre, direction III) barely shows any residual strength due to the fact that the fibres do not bridge the layer interface. Nevertheless, the failure behaviour is slightly less brittle than that of the printed specimens without fibres (direction I) (cf. $f_{R1*0.27}$ values). The cause is difficult to identify. Possibly the presence of fibres around the fracture surface nevertheless increase the resistance.

The series printed in direction I with FF15E0 fibres clearly performs better than both the printed specimens in direction III and then the cast specimens. For these specimens, the fibres are oriented in the favourable direction, which results both in a higher crack strength, and a higher post-peak behaviour. At $f_{R1*0.27}$ a considerably residual strength of 3.70 MPa is left. However, at $f_{R3*0.27}$ only 0.90 MPa remains. This is due to the failure mode of the fibres. Rather than failing by pull-out, they fail by breakage. This is enabled by the high ratio of surface to cross-sectional area, which results in a relatively strong bond between the fibre and the matrix. Although the overall performance is decidedly less brittle than that of the printed specimens without fibres (direction I), or the printed specimens with FF15E0 fibres in direction III, the residual strength still reduces too swiftly to allow a classification according to the *fib* Model Code 2010 ('<a').

The performance of the printed specimens with Cem-FIL fibres is pointedly different. The glass fibres do not significantly increase the cracking strength but do result in a considerable increase in ductility (cf. $f_{R1*0.27} \approx f_{R3*0.27}$), resulting in a classification 'c'. Contrary to the FF15E0 fibres, the Cem-FIL specimens fail by fibre pull-out, rather than fibre breakage which is much more abrupt.

From showing that the developed method allows printing of reasonably ductile fibre-reinforced mortar, as well as brittle unreinforced mortar, it may be concluded that the application of this OD-FG strategy with the use of the PTS and PAD devices is promising to grade structural strength and ductility (in direction I) by location. It also shows the possibility to influence the structural behaviour by adding different kinds of fibres.

4.2.4 Density

A rectangular object was printed, as shown in Figure 8. Initially, the PTS and PAD devices were set to achieve a maximum addition of lightweight aggregates. In two steps, the particle addition was decreased to 0, by reducing the power supply to the blower motor of the PTS (see also Figure 2(b)). Thus, specimens 1–3

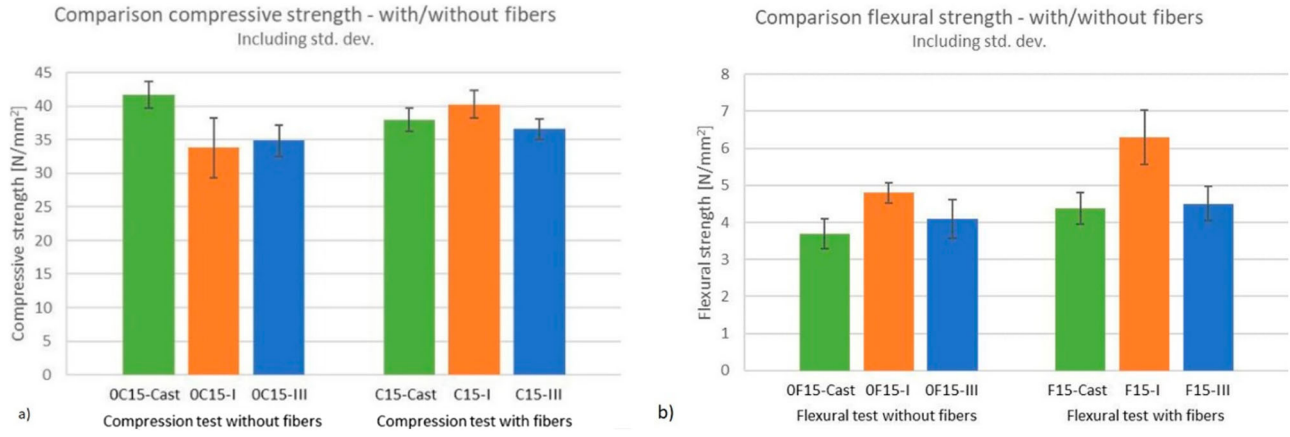

Figure 6. (a) Results from Compression test-with and without fibres, (b) results from the flexural bending tests- with and without fibres.

had the lowest density, 4–6 an intermediate density, and 7–8 the base material density.

The average densities of specimen series are given in Table 7. The top part of the table shows densities of normal weight specimen series, while the bottom part shows the results of the step-wise experiment with the lightweight aggregates. The table shows that the influence of fibres on the specimen weight is negligible. The expanded glass aggregate, on the other hand, noticeably reduces the overall density, as a function of the quantity of aggregate that is added. At the maximum, an average reduction of 14.3% was obtained compared to printed concrete in direction I without particles. In the intermediate setting, this reduced to a 7.1% reduction. At the final setting, the difference obviously disappeared entirely as no lightweight aggregate was applied anymore. Photographs of the samples (Figure 9 (a–h)) clearly show the decreasing quantity of aggregates, which corresponds with an increasing average density.

5. Experimental evaluation of functional grading with (RPS): in between the layers

5.1. Methods

The second grading strategy was applied by depositing fibres in between layers of printed filament. A trial tested showed that the Fibraflex FF15E0 fibre disastrously reduced the bond between filament layers, due to its relatively large surface area (Figure 10(b,c)). Therefore the experiment was conducted with Cem-FIL Minibars 24 mm fibres only, as it was the only remaining fibre type to meet all requirements. Using the PTS, the fibres were transported to the print head, but rather than injecting them into the PAD, the splitter exit was connected to a short pipe held by a clamp that maintained its position 150 mm in front of the nozzle and 250 mm above the previously printed surface (Figure 10(a)). The lack of rotation capacity of the fibre depositing pipe means that at this stage of development, the strategy can only be applied to straight print paths.

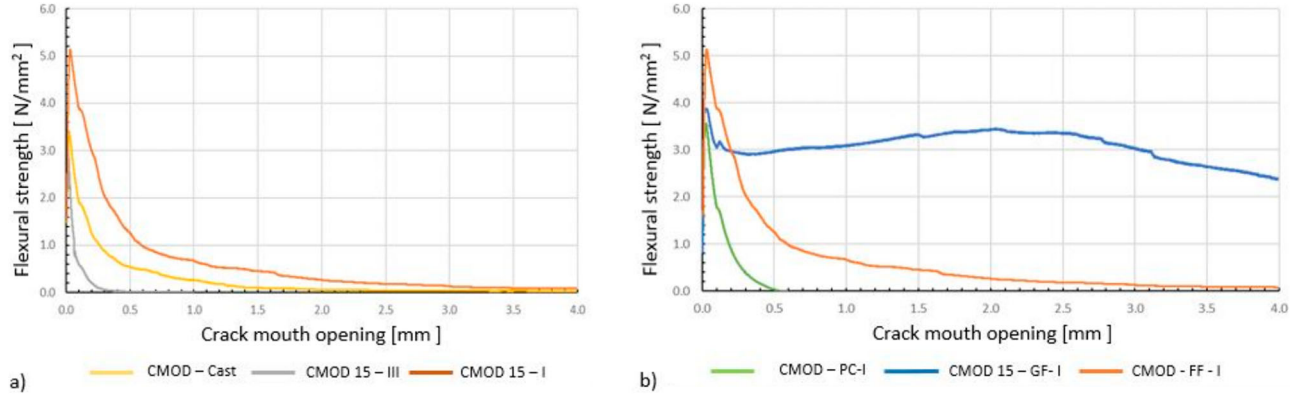

Figure 7. (a) Average results from the CMOD tests; influence of orientation in FF15E0 fibre reinforced concrete, (b) Average results from the CMOD tests; influence of fibre type (PC = plain concrete vs GF = CEM FIL minibars glass fibre vs FF = Fibraflex FF15E0 steel fibre).

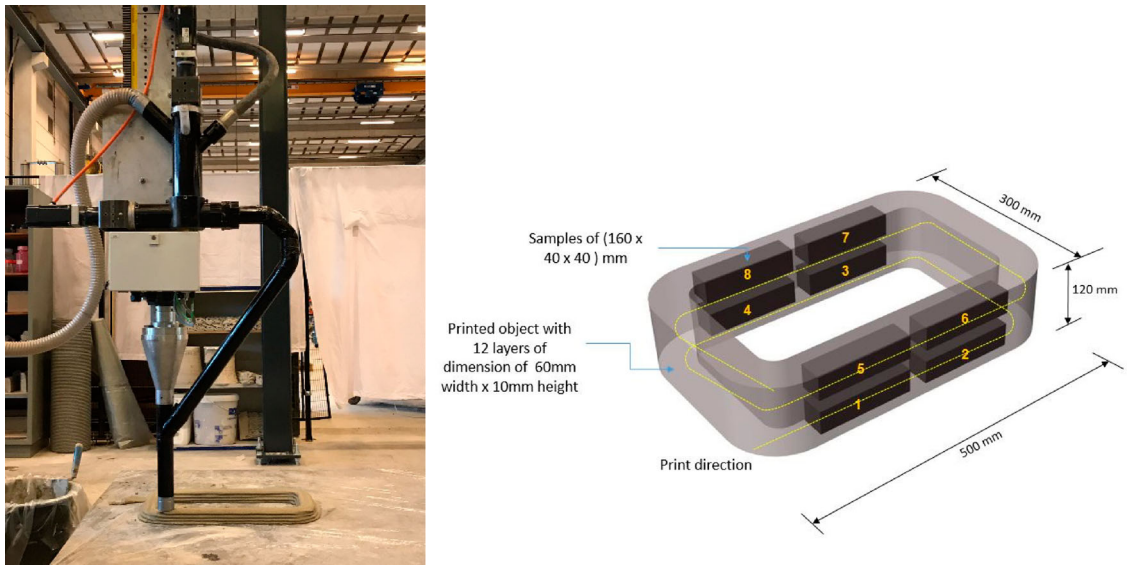

Figure 8. Printed object for gradual grading of density by steadily reducing the input of light weigth aggregates. The specimens 1 through 8 were extracted from the indicated locations in the object.

The settings detailed in Section 4.1 were used, except for the water/mortar ratio which for this process was kept at 0.15 (which is default water/mortar ratio for [anonymous] setup) because sprinkling fibres on top of the printed layers does not affect the workability of the printed concrete.

As no earlier data on the mechanical performance of mortars with layer-wise fibre reinforcement exist, a

Table 5. Results of flexural test.

Production and orientation	Fibre	Number of specimens	Age at testing	Average flexural strength (rel. stand. dev.)	Results of Wolfs, Bos, and Salet 2019 (age)
Cast	None	5	13 days	3.7 MPa (10.9%)	4.3 (7 days)
Printed, dir. I	None	10	13 days	4.8 MPa (5.7 %)	4.3 (7 days)
Printed, dir. III	None	10	13 days	4.1 MPa (12.6 %)	3.7 (7 days)
Cast	FF15E0	5	13 days	4.4 MPa (9.8 %)	–
Printed, dir. I	FF15E0	10	13 days	6.3 MPa (11.6 %)	–
Printed, dir. III	FF15E0	10	13 days	4.5 MPa (10.3 %)	–

Table 6. Results of CMOD test.

Production and orientation	Fibre	Number of specimens	Age at testing	Average cracking strength f_t (RSD)	Scaled CMOD properties* $f_{R1*0.27}$	$f_{R3*0.27}$	$f_{R3*0.27}/f_{R1*0.27}$	Classification
Cast	FF15E0	5	13 days	3.4 MPa (12.6 %)	1.7 MPa	0.44 MPa	0.26	<a
Printed, dir. I	FF15E0	5	13 days	4.6 MPa (8.3 %)	3.7 MPa	0.90 MPa	0.25	<a
Printed, dir. III	FF15E0	5	13 days	2.9 MPa (7.1 %)	0.38 MPa	0.00 MPa	0.00	<a
Printed, dir. I	none	5	13 days	4.0 MPa (17.5 %)	1.1 MPa	0.00	0.00	<a
Printed, dir. I	Cem-FIL mb 24 mm	5	13 days	4.2 MPa (8.9 %)	3.1 MPa	3.0 MPa	0.99	c

Table 7. Densities of different samples.

Production and orientation	Particle	Number of specimens	Average density (rel. stand. dev.)
Cast	None	7	2183 kg/m^3 (2.5%)
Cast	FF15E0	5	2169 kg/m^3 (2.0%)
Printed, dir. I	none	8	2117 kg/m^3 (1.4%)
Printed, dir. I	FF15E0	10	2222 kg/m^3 (1.4%)
Printed, dir. III	FF15E0	10	2143 kg/m^3 (1.9%)
Printed, dir. I	Cem-FIL mb 24 mm	8	2105 kg/m^3 (0.6%)
Printed, dir. I	Liaver aggregates, maximum	3 (1, 2, 3)	1816 kg/m^3 (1.8%)
Printed, dir. I	Liaver aggregates, intermediate	3 (4, 5, 6)	1969 kg/m^3 (0.5%)
Printed, dir. I	Liaver aggregates, minimal (none)	2 (7, 8)	2152 kg/m^3 (1.5%)

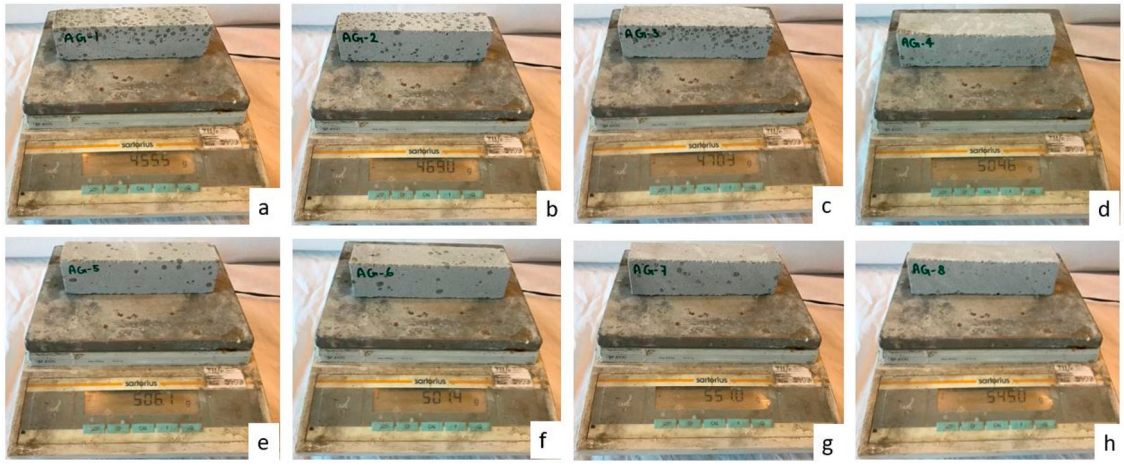

Figure 9. Specimens from density grading experiment. (a–c) Samples 1, 2, 3 with a maximum quantity of lightweight aggregates, (d–f) samples 4, 5, 6, with an intermediate quantity, (g, h) samples without lightweight aggregates.

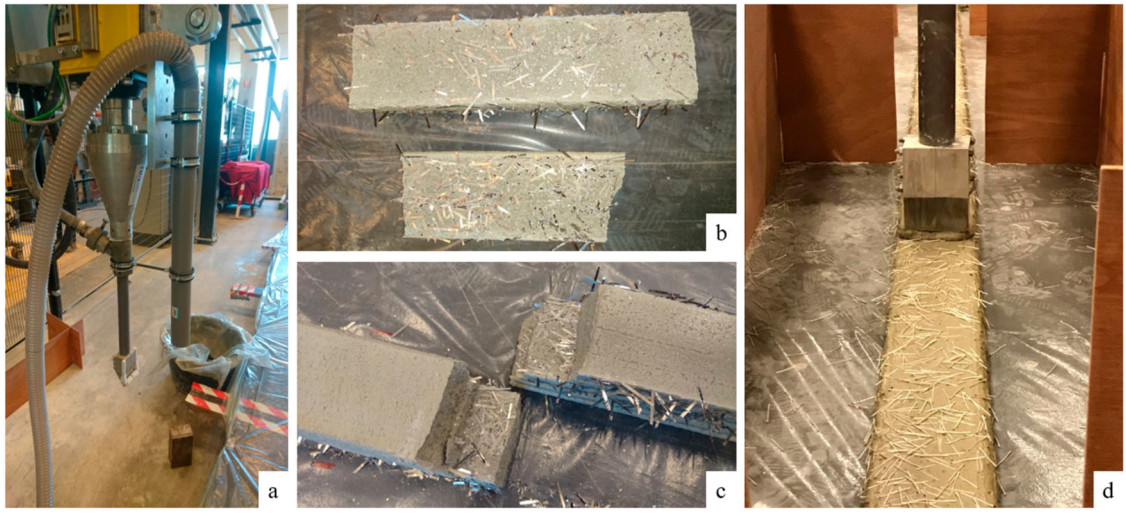

Figure 10. Repetitive sequential Process (RPS) (a) nozzle connection with PTS hose, (b, c) poor interface layer with FF15E0 fibres, (d) sample printed with CEM-FIL minibar 24 mm fibres.

target fibre quantity was difficult to formulate from a structural performance perspective. Integrating quantities from in-bulk fibre-reinforced mortar to a quantity per surface area results in amounts that could not be transported with the PTS system, and would furthermore likely cause serious reductions of the perpendicular interface strength. Therefore, the transportable quantity from the PTS was considered as a given and a first indication of the performance that would be achievable. On average, this corresponded with 1.2 VOL% of fibres with the current filament dimensions.

Unlike the SP, the orientation of the fibres for this strategy of printing were random in XY direction, due to the sprinkling of fibres. If some fibres got overlapped on to one another it did not have any major influence in the printed layers during the printing process. However, some fibre types got collected in front of the nozzle (Figure 10(d)) after a period of printing. The CEM Fil fibres were least prone to this effect.

The ductility of the printed specimens, with this strategy is validated by performing CMOD tests on the specimens prepared as described in Section 4.1.

5.2. Results and discussion

Table 8 gives an overview of the results of the CMOD test. The average cracking strength is somewhat low compared to the results presented in Section 4.2.3. On average, the post-peak strength is insufficient to warrant a classification according to the *fib* Model Code 2010. However, with a relative standard deviation of 70%, the scatter in results in very high. This is due to the variation in the number of fibres found in the fracture surface, ranging from 6 to 0. Thus the results are equally

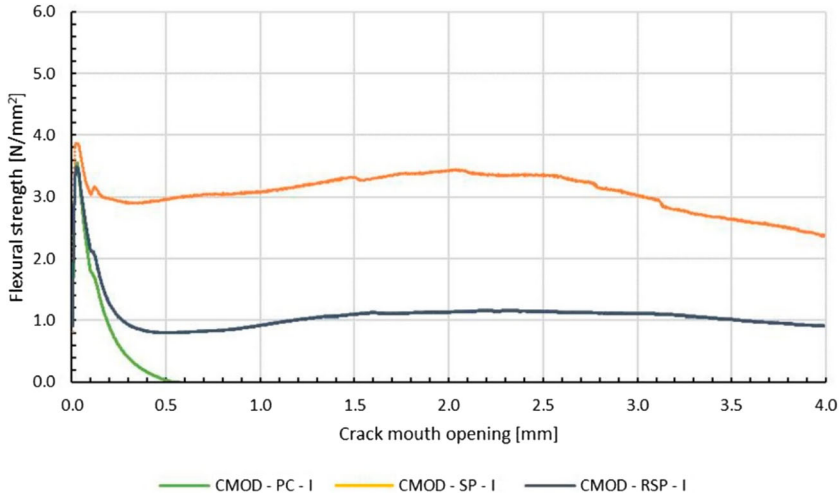

Figure 11. Average results from the CMOD tests comparing results for plain concrete vs CEM FIL minibars 24 mm fibres with SP (using PTS+PAD) vs CEM FIL minibars 24 mm fibres with RSP process (using PTS).

Table 8. Results of CMOD test.

Production and orientation	Fibre	Number of specimens	Age at testing	Average cracking strength f_t (RSD)	Scaled CMOD properties*			
					$f_{R1*0.27}$	$f_{R3*0.27}$	$f_{R3*0.27}/f_{R1*0.27}$	classification
Printed, dir. I	Cem-FIL mb 24 mm	8	9 days	3.7 MPa (15.9%)	1.7 MPa	0.72 MPa	0.42	<a

widespread, with hardly any ductility for specimen #8, but $f_{R3*0.27} > f_{R1*0.27}$ for specimen #1. In cases where there are fibres, the ductility achieved is considerable – better than for the specimens with FF15E0 fibres produced according to the SP (strategy 1, Section 4.2.3). This is due to the failure behaviour of the fibres. The residual strength of printed specimens applying the RSP (this strategy) could be improved by increasing the layer width-to-height ratio.

6. Summary and conclusions

Two strategies were presented to achieve functional grading in extrusion-layering 3D concrete printing. The first is based on the selective addition of particles (fibres, aggregates, etc.) to the print mortar in a 2nd-stage mixing process at the print head. The second is based on the addition of particles in between the layers of printed concrete. The designs of two devices as addition to an existing 3D concrete printing facility with which the strategies can be realised were discussed. The Particle Transportation System (PTS) is an airborne system to continuously transport discrete particles to the print head, which is used in both strategies. The Particle Addition Device (PAD) is a 2nd-stage mixing device attached to the print head, specifically for use with strategy 1.

Trials were performed to develop the equipment and test operability. Subsequently, specimens were printed according to strategies 1 and 2 with different fibres and a lightweight aggregate, and subsequently (mechanically) tested to provide a proof-of-concept that the developed equipment could achieve meaningful functional performance differences in printed concrete.

The trials showed that an airborne system is suitable to transport a variety of particles to the print head, including fibres and lightweight aggregates. Calibration per particle type remains necessary and alignment of the transported particle quantity with the required quantity at printer head need to be improved. The developed mixing system (PAD) is also compatible with the current 3D concrete printing facility. Test trials showed that in general a homogeneous distribution of particles is found at the printer nozzle. Also for this system, it is necessary to calibrate the settings per particle type, this is because the type and quantity highly affects the workability of the material and thus the required settings of the system.

Applying strategy 1 in combination with the appropriate type of fibre can result in promising improvements in ductility. With further optimisations of the technology, pseudo-elasto-plastic failure behaviour in direction I (direction of printing) may be achieved. Further improvements to the technology seem necessary to achieve meaningful weight reductions through the addition of lightweight aggregates (i.e. the system should be capable to add a higher VOL% of aggregates).

To achieve post-fracture ductility in 3D printed concrete, Cem-FIL minibars 24 mm glass fibres perform significantly better than Fibraflex FF15E0 steel fibres, due to their failure mode (pull-out versus breakage). Out of all the test conducted for both the system, only CMOD test with CEM FIL minibar 24 mm can be compared for both the production process – as shown in Figure 11.

Although the second strategy has the distinct advantage that no additional aggregates have to be added to the print mortar, it is difficult to achieve relevant increases in ductility with fibres as this needs a considerable amount of fibres in the interlayer surface (limited by bond reduction between layers) as well as an even distribution (to avoid failures at the weakest link).

Acknowledgements

The support of the staff of the Structures Laboratory Eindhoven is gratefully acknowledged. The support of Ph.D. students Lauri Hass and Rob Wolfs, and the assistance in the 3DCP research of Master track students Structural Design at the TU/e Department of the Built Environment is highly valued. For this paper, the authors appreciate the work of I.H.A. Geurts, V.N.A. Hoedemakers, L. Louer, and E.M. van den Tillaart in particular, for their assistance in the experimental work. The TU/e research programme on 3D Concrete Printing is co-funded by a partner group of enterprises and associations, that on the date of writing consisted of (alphabetical order) Ballast Nedam, BAM Infraconsult bv, Bekaert, Concrete Valley, CRH, Cybe, Saint-Gobain Weber Beamix, SGS Intron, SKKB, Van Wijnen, Verhoeven Timmerfabriek, and Witteveen+Bos. Their support is gratefully acknowledged.

Disclosure statement

No potential conflict of interest was reported by the authors.

Notes on contributors

Zeeshan Yunus Ahmed completed his master's in Architectural Design from Bartlett, University College London, and is currently a Ph.D. student in the Department of Built Environment, Eindhoven University of Technology (TU/e). His research is focused on digital design and manufacturing of 3d concrete printed (3DCP) structures. Key research topics include developing entrainment processes for reinforcing 3DCP structures and developing large-scale application 3DCP with valorisation projects such as 3d concrete printed bridge at Gemert (Netherlands), Project milestone(3DCP houses in Eindhoven), and 3DCP bridge at Nijmegen.

Freek Bos is an Assistant Professor of Concrete Structures in the Department of the Built Environment, Eindhoven University of Technology (TU/e). His research in the field of Additive Manufacturing of Cementitious materials focuses on reinforcement concepts for 3D Concrete Printing. Key ongoing research topics include online entrained cable reinforcement, as well as the development of printable Strain-Hardening Cementitious Composites. Freek is a member of the RILEM TC 276 Digitally Fabricated Concrete and the *fib* TG 2.11 Digital Concrete.

Maikel van Brunschot completed his master's in structural design from Eindhoven University of Technology. Focusing his graduation topic on the possibility to implement fibre reinforcement in 3DCP. Currently, he is working as a structural engineer in the field of concrete structures, predominantly on the design and optimisation of precast concrete elements.

Theo Salet is Dean of the Department of the Built Environment and Full Professor of Structural Design/Concrete Structures. Ever since the start of his international engineering career the focus of the work of Theo Salet is on numerical simulations, amongst hardening concrete. He has worked on a variety of noteworthy bridges, tunnels and buildings. At TU/e, the focus of his research is on the integration of design and construction in concrete. For the early design phase, structural models are developed and validated, best described as 'Parametric Design Tools'. For later design phases including product development he applies and develops advanced non-linear elastic finite element models for concrete: 'Numerical Concrete'. His research is constantly linked to research of practical applications of new and 'high-tech' concrete. A notable research subject is his work on 3D-printed (fibre) reinforced concrete. The research group operates and further develops its own 3D concrete printer. Here, Salet's research focuses – amongst others – on the issue of the robustness of the print process and the opportunities to embed reinforcement during the print process to enable structural applications.

ORCID

Z.Y. Ahmed http://orcid.org/0000-0001-7250-9752
F.P. Bos http://orcid.org/0000-0002-6666-2395

References

Altenhofen, C., T. H. Luu, T. Grasser, M. Dennstädt, J. S. Mueller-Roemer, D. Weber, and A. Stork. 2018. "Continuous Property Gradation for Multi-material 3d-Printed Objects." Solid freeform fabrication 2018: proceedings of the 29th annual international solid freeform fabrication symposium – an additive manufacturing conference.

Aouf, R. S. 2018, September 5. "US Military 3D Prints Concrete Barracks on Site." Dezeen: https://www.dezeen.com/2018/09/05/us-military-3d-prints-concrete-barracks-on-site-technology/.

Aouf, R. S. 2019, July 24. "Students' 3D-Printed Concrete Choreography Pillars Provide a Stage for Dancers." Dezeen: https://www.dezeen.com/2019/07/24/3d-printed-concrete-choreography-pillars-design/.

Asprone, D., C. Menna, F. Bos, T. Salet, J. Mata-Falcón, and W. Kaufmann. 2018, October. "Rethinking Reinforcement for Digital Fabrication with Concrete." *Cement and Concrete Research* 112: 111–121.

Audibert, C., J. C. Jacob, J. M. Linares, and Q. A. Lopez. 2018, December 15. "Bio-Inspired Method Based on Bone Architecture to Optimize the Structure of Mechanical Workspieces." *Materials & Design* 160: 708–717.

Bao, Y., M. Xu, D. Soltan, and T. Xia. 2018. "Three-Dimensional Printing Multifunctional Engineered Cementitious Composites (ECC) for Structural Elements." *First RILEM International Conference on Concrete and Digital Fabrication – Digital Concrete 2018* 19: 115–128.

Bever, M., and P. Duwez. 1972. "Gradients in Composite Materials." *Materials Science and Engineering* 10: 1–8.

Bos, F. P., E. Bosco, and T. A. Salet. 2019. "Ductility of 3D Printed Concrete Reinforced with Short Straight Steel Fibers." *Virtual and Physical Prototyping* 14 (2): 160–174.

Bos, F. P., R. J. Wolfs, Z. Y. Ahmed, and T. A. Salet. 2016. "Additive Manufacturing of Concrete in Construction: Potentials and Challenges of 3D Concrete Printing." *Virtual and Physical Prototyping* 11 (3): 209–225.

Camacho, D. D., P. Clayton, W. J. O'Brien, C. Seepersad, M. Juenger, R. Ferron, and S. Salamone. 2018. "Applications of Additive Manufacturing in the Construction Industry – A Forward-Looking Review." *Automation in Construction* 89: 110–119.

Cem-fil Minibars data sheet. n.d. September 9, 2019, Ownes Corning: http://www.ocvreinforcements.com/pdf/library/10021900_Cem_FIL_MiniBars_product_sheet_ww_01_2018_Rev1_EN.pdf.

Cho, W., E. M. Sachs, N. M. Patrikalakis, M. J. Cima, H. Liu, J. Serdy, and C. C. Stratton. 2002. "Local Composition Control in Solid Freeform Fabrication." *Service and Manufacturing Grantees and Research Conference*. San juan, puerto rico.

Craveiro, F., H. M. Bartolo, A. Gale, J. P. Duarte, and P. J. Bartolo. 2017. "A Design Tool for Resource-Efficient Fabrication of 3d-Graded Structural Building Components Using Additive Manufacturing." *Automation in Construction* 82: 75–83.

Craveiro, F., H. Bártolo, and P. Bártolo. 2013. "Functionally Graded Structures Through Building Manufacturing." *Advanced Materials Research* 683: 775–778.

Declaration of performance. n.d. September 9, 2019, Fibraflex: http://www.fibraflex.fr/sites/fibraflex.com/files/pdf/qfa-ddp-ffx-en.pdf.

Duballet, R., C. Gosselin, and P. Roux. 2015. "Additive Manufacturing and Multi-Objective Optimization of Graded Polystyrene Aggregate Concrete Structures." In *Modelling Behaviour*, edited by M. Thomsen, M. Tamke, C. Gengnagel, B. Faircloth, and F. Scheurer, 225–235. Cham: Springer International Publishing.

Fibraflex Brochure. (n.d.). September 8, 2019, FibraFlex: http://www.fibraflex.fr/sites/fibraflex.com/files/pdf/ffx_brochure-uk_versionelectronique_pl.pdf.

Garland, A. P., and G. Fadel. 2015. "Design and Manufacturing Functionally Gradient Material Objects With an Off the Shelf Three-Dimensional Printer: Challenges and Solutions." *Journal of Mechanical Design* 137: 11.

International Federation for Structural Concrete (fib). 2013. *fib Model Code for Concrete Structures 2010*. Lausanne: Ernst & Sohn.

Jordahn, S. 2018, November 19. "Arup and CLS Architetti's 3D-Printed House was Built in a Week." Dezeen: https://www.dezeen.com/2018/11/19/video-mini-living-3d-printing-cls-architetti-arup-movie/?li_source=LI&li_medium=rhs_block_1.

Khoshnevis, B. 2004. "Automated Construction by Contour Crafting – related Robotics and Information Technologies." *Automation in Construction* 13 (1): 5–19.

Khoshnevis, B., R. Russell, H. Kwon, and S. Bukkapatnam. 2001. "Contour Crafting – a Layered Fabrication Technique." *Special Issue of IEEE Robotics and Automation Magazine* 8 (3): 33–42.

Khosnhevis, B., D. Hwang, K.-T. Yao, and Z. Yeh. 2006. "Mega-Scale Fabrication by Contour Crafting." *International Journal of Industrial and Systems Engineering* 1 (3): 301–320.

Kirk, T., E. Galvan, R. Malak, and R. Arróyave. 2018. "Computational Design of Gradient Paths in Additively Manufactured Functionally Graded Materials." *Journal of Mechanical Design* 140: 11.

Leung, Y.-S., H. Mao, and Y. Chen. 2018. "Approximate Functionally Graded Materials for Multi-Material Additive Manufacturing." *ASME 2018 International Design Engineering Technical Conferences and Computers and Information in Engineering Conference*. doi:10.1115/DETC2018-86391.

Liaver balls Brochure. n.d. September 9, 2019, Liaver Expanded Glass Technology: http://www.liaver.com/fileadmin/user_upload/pdf/Liaver_reapor_en.pdf.pdf.

Lim, S., R. A. Buswell, T. T. Le, S. A. Austin, A. G. Gibb, and T. Thorpe. 2012. "Developments in Construction-Scale Additive Manufacturing Processes." *Automation in Construction* 21: 262–268.

Lindemann, H., R. Gerbers, S. Ibrahim, F. Dietrich, E. Herrmann, K. Dröder, and H. Kloft. 2018. "Development of a Shotcrete 3D-Printing (SC3DP) Technology for Additive Manufacturing of Reinforced Freeform Concrete Structures." *First RILEM International Conference on Concrete and Digital Fabrication – Digital Concrete 2018* 19: 287–298.

Lloret, E., A. Shahab, M. Linus, R. Flatt, F. Gramazio, K. Matthias, and S. Langenberg. 2015, March. "Complex Concrete Structures: Merging Existing Casting Techniques with Digital Fabrication." *Computer-Aided Design* 60: 40–49.

Lowke, D., E. Dini, A. Perrort, D. Weger, C. Gehlen, and B. Dillenburger. 2018, October. "Particle-bed 3D Printing in Concrete Construction – Possibilities and Challenges." *Cement and Concrete Research* 112: 50–65.

Maalej, M., S. F. Ahmed, and P. Paramasivam. 2003. "Corrosion Durability and Structural Response of Functionally-Graded Concrete Beams." *Journal of Advanced Concrete Technology* 1 (3): 307–316.

Material district. 2019, May 23. "New Record for Longest 3d Printed Concrete Pedestrian Bridge in the World." Material District: https://materialdistrict.com/article/record-longest-3d-printed-concrete-pedestrian-bridge/.

Mensley, M. 2017, June 2. "Dubai's New Drone Laboratory is 3D Printed from Concrete." June 2, 2017, All3DP: https://all3dp.com/concrete-3d-printing-dubai-drone-lab/.

Mohamed, M., and V. Li. 1995, March 1. "Introduction of Strain-Hardening Engineered Cementitious Composites in Design of Reinforced Concrete Flexural Members for Improved Durability." *International Concrete Abstracts Portal* 92 (2): 167–176.

Mohammad, V., S. Chianrabutra, B. Mellor, and S. Yang. 2013. "Multiple Material Additive Manufacturing – Part 1: A Review." *Virtual and Physical Prototyping* 8: 19–50.

NEN-EN 12390-3:2009 EN. 2009. *Testing Hardened Concrete - Part 3: Compressive Strength of Test Specimens*. Delft: Nederlands Normalisatie Instituut.

NEN-EN 14651:2005 EN. 2005. *Test Method for Metallic Fibered Concrete - Measuring the Flexural Tensile Strength (Limit of Proportionality (LOP), Residual)*. Delft: Nederlands Normalisatie Instituut.

Oxman, N., S. Keating, and E. Tsai. 2011. "Functionally Graded Rapid Prototyping." *Proceedings of VRAP: Advanced research in Virtual and Rapid Prototyping*.

Plückelmann, S., F. Song, and R. Breitenbücher. 2017. "Hybrid Concrete Elements with Splitting Fiber Reinforcement Under Two-Dimensional Partial Area Loading." In *High Tech Concrete: Where Technology and Engineering Meet*, edited by D. Hordijk and M. Luković, 347–355. Springer.

Ramela. (n.d.). September 12, 2019, http://www.ramella.com/picker.php

Salet, T. A., Z. Y. Ahmed, F. P. Bos, and H. L. Laagland. 2018. "Design of a 3D Printed Concrete Bridge by Testing." *Virtual and Physical Prototyping* 13 (3): 222–236.

Shen, M., and M. Bever. 1972. "Gradients in Polymeric Materials." *Journal of Material Sciences* 7 (7): 741–746.

Shen, B., M. Hubler, G. H. Paulino, and L. J. Struble. 2008. "Functionally-Graded Fiber-Reinforced Cement Composite: Processing, Microstructure, and Properties." *Cement and Concrete Composites* 30 (8): 663–673.

Tay, Y. W., B. Panda, S. C. Paul, N. A. Mohamed, M. J. Tan, and K. F. Leong. 2017. "3D Printing Trends in Building and Construction Industry: A Review." *Virtual and Physical Prototyping* 12 (3): 261–276.

Uygar endustri. n.d. September 12, 2019, https://www.uygarendustri.com.tr/en/products/fiber-dosing-systems.

Wangler, T., N. Roussel, F. P. Bos, T. A. Salet, and R. J. Flatt. 2019. "Digital Concrete: A Review." *Cement and Concrete Research* 123.

Wolfs, R. J., F. P. Bos, and T. A. Salet. 2019. "Hardened Properties of 3D Printed Concrete: The Influence of Process Parameters on Interlayer Adhesion." *Cement and Concrete Research* 119: 132–140.